Rare Metal Materials and Engineering
Volume 55, Issue 7, July 2026
Available online at www.rmme.ac.cn

Science Press

Cite this article as: Zhao Xingchi, Li Ruixue, Li Penghao, et al. Influence of Ce Addition on Microstructure and Properties of 1060 Current Collector Battery Aluminum Foil[J]. Rare Metal Materials and Engineering, 2026, 55(07): 1664-1672. DOI: https://doi.org/10.12442/j.issn.1002-185X.20250416.

ARTICLE

Influence of Ce Addition on Microstructure and Properties of 1060 Current Collector Battery Aluminum Foil

Zhao Xingchi[1,2], Li Ruixue[1], Li Penghao[3], Li Wanying[4], Li Jilin[1,2], Jiang Bo[1], Du Xinwei[5]

[1] School of Materials Science and Chemical Engineering, Harbin University of Science and Technology, Harbin 150080, China; [2] Institute of New Materials, Guangdong Academy of Sciences, Guangzhou 510640, China; [3] School of Information Engineering, Guangzhou International Economics College, Guangzhou 510540, China; [4] Guangzhou Yiyin New Material Technology Co., Ltd, Guangzhou 510640, China; [5] Ruyuan Dongyangguang UACJ Fine Aluminum Foil Co., Ltd, Shaoguan 512600, China

Abstract: Commercially applied 1060 current collector battery aluminum foil was selected as the base material for the addition of rare-earth element Ce. Melting, degassing, filtration, hot rolling, and cold rolling processes were conducted on the Ce-added aluminum foil. The influence of Ce addition on the 1060 current collector battery aluminum foil was analyzed. Results indicate that AlCeSi intermetallic phases are generated in the 1060 current collector battery aluminum foil and act as heterogeneous nucleation sites, therefore refining the grains. In the cold rolling deformation process, the Ce-containing secondary phase particles at the grain boundary produces a strong Zener pinning effect, increases the dislocation density, and inhibits the recrystallization. Consequently, the mechanical properties of the aluminum foil are enhanced through the synergistic actions of grain refinement strengthening and dislocation strengthening. Ce addition also reduces the impurity element solubility in the matrix, modifies lattice distortion scattering, and therefore enhances electrical conductivity. Adding the rare-earth element Ce can refine grains and promotes the positive shift of corrosion potential, thereby improving the corrosion resistance.

Key words: current collector battery aluminum foil; micro-Ce alloying; rolling process; electrical conductivity; corrosion resistance

1 Introduction

With the rapid development of new energy vehicles and the energy storage market, the development of the new energy battery industry is urgent and important. Among all sorts of batteries, the lithium battery is the main representative, and new batteries, such as solid-state batteries, sodium-ion batteries, and fuel cells, are gradually developed and improved. According to the development and application trend of global new energy batteries, it is inferred that the demand for global lithium batteries will reach 4 T·W·h by 2030. As a positive current collector material, aluminum foil is responsible for carrying active substances and transmitting current in lithium batteries[1]. Aluminum foil stands out from other metals because of its low density, good mechanical properties, and fine electrical conductivity[2–3]. In addition, the chemical potential of aluminum is lower than that of most electrolytes, so it can avoid the reduction of electrolytes[4]. The evolving battery industry imposes stringent requirements on aluminum foil current collectors: (1) high electrical conductivity, which ensures the rapid transfer of electrons inside the electrode; (2) good corrosion resistance, which ensures serving safty during the long-term charge and discharge cycles (corrosive condition); (3) high strength and toughness; (4) high thermal electrical conductivity, which ensures quick conduction of the ohmic heat and chemical reaction heat inside the battery[5–8].

At present, the current collector battery aluminum foil mainly uses 1XXX series aluminum alloys, such as 1060, 1080, and 1100 alloys[7]. However, due to their low strength and inferior corrosion resistance, the growing performance requirements of lithium-ion batteries cannot be satisfied. It is

Received date: August 08, 2025
Corresponding author: Li Jilin, Ph. D., Professor, Institute of New Materials, Guangdong Academy of Sciences, Guangzhou 510640, P. R. China, Tel: 0086-20-87716056, E-mail: Li197307@163.com; Jiang Bo, Ph. D., Professor, School of Materials Science and Chemical Engineering, Harbin University of Science and Technology, Harbin 150080, P. R. China, E-mail: jiangbo@hrbust.edu.cn; Du Xinwei, Ruyuan Dongyangguang UACJ Fine Aluminum Foil Co., Ltd, Shaoguan 512600, P. R. China, E-mail: duxinwei2000@126.com

necessary to develop a high-performance current collector battery aluminum foil.

In recent years, rare-earth (RE) elements have been widely used in aluminum alloys. Extensive studies have reported that RE elements exhibit potent degassing capability during the smelting of aluminum alloy. By effectively reducing the hydrogen content in the melt, RE additions thereby mitigate gas pore formation in the final solidified alloy. Simultaneously, RE elements serve as efficient modifiers that refine the microstructure by altering the solidification path, ultimately enhancing the mechanical properties of the aluminum alloy[9–13]. For example, Cui et al[14] studied the refinement and modification mechanisms of RE element Ce on Al-7%Si-0.6%Mg casting alloy. The results show that the addition of 0.1%–0.2% Ce can form the AlCeSi phase, which acts as a heterogeneous nucleation core to reduce the average grain size of α-Al from 80.44 μm to 47.21 μm and refines the eutectic silicon by increasing the undercooling temperature range (ΔT) of the alloy (ΔT increases from 0.65 ℃ to 1.78 ℃). The alloy morphology changes from flake to fibrous type. In addition, the adsorption of Ce atoms on the surface of eutectic silicon induces high-density stacking faults, which further promote the modification of eutectic silicon and inhibit the growth of the iron-rich phase, thereby improving the microstructure and mechanical properties of the alloy. Li et al[15] studied the effect of RE element La on the microstructure and mechanical properties of as-cast Al-5.4Cu-0.7Mg-0.6Ag alloy. It was found that trace La could significantly refine α-Al grains. When the content of La was 0.4wt%, the mechanical properties of the La-added alloy at room temperature and 350 ℃ were better than those of the alloy without La addition. RE elements can also improve the corrosion resistance of the alloy. Yu et al[16] studied the effect of La content on the microstructure, mechanical properties, electrical conductivity, and corrosion behavior of as-cast Al-0.5wt% Fe alloy. The research conclusions are as follows: La significantly refines the grain and changes the morphology of the Fe-containing phase, but it has a restricted influence on the strength. The elongation and electrical conductivity increase firstly and then decrease. Besides, the corrosion resistance of the alloy is also enhanced. When the La content is 0.10wt%, the elongation and electrical conductivity are further imporved. In addition, RE elements can also improve the electrical conductivity of aluminum alloys. An appropriate addition amount of RE elements can reduce the thermal expansion coefficient of the alloy and increase the thermal electrical conductivity. Numerous studies indicate that Ce and La impart comparable beneficial effects on the microstructure and mechanical properties of aluminum alloys. Addition of Ce or La into aluminum alloy conductors can effectively modify the as-cast microstructure and promote grain refinement[17–18]. Moreover, Ce and La can also form intermetallic compounds with the main impurity elements, such as Fe and Si, in industrially pure aluminum, reducing the concentration of solid solution atoms in the aluminum matrix, and thereby increasing the electrical conductivity of the alloy[19–21].

In this research, trace RE element Ce was added into the 1060 current collector battery aluminum foil by the element microalloying method to improve the performance. The effects of Ce addition on the microstructure and properties of 1060 current collector battery aluminum foil were studied through tensile test, electrical conductivity test, and electrochemical test.

2 Experiment

The chemical composition of the aluminum foil used in this study is shown in Table 1. The raw material and Ce-added material are denoted as 1# and 2# samples, respectively. The experiment samples were prepared using high-purity aluminum ingots. Alloying elements (Si, Fe, and Ce) were introduced into master alloys: Al-20Si, Al-20Fe, and Al-15Ce. High-purity aluminum ingots were melted at 780 ℃ in graphite crucibles. The intermediate alloys were submerged at 730 ℃ and stirred for 5 min to ensure uniform composition. The hexachloroethane refining agent was used to remove gas and slag, and the casting was conducted after holding at 720 ℃ for 20 min. According to the process flow in Fig.1, the aluminum alloy ingots were homogenized in a box-type resistance furnace. After homogenization at 580 ℃ for 8 h, the samples underwent furnace cooling. Hot rolling was performed on an LG500 mill at 500 ℃ for 120 min, reducing the thickness to 2.8 mm. The hot-rolled blank underwent intermediate annealing at 500 ℃ for 150 min. Subsequent cold rolling on a four-high mill produced foils of 1060 and 1060-0.05Ce samples with thickness of 0.3 mm, which are designated CR-1# and CR-2#, respectively. Then, the CR-1# and CR-2# foils underwent low-temperature annealing at 200 ℃ for 6 h, yielding final products CR-LA-1# and CR-LA-2#, respectively.

Table 1 Chemical composition of 1060 and 1060-0.05Ce alloys (wt%)

Sample	Si	Fe	Cu	Mn	Mg	Zn	Ti	V	Ce	Al
1#	0.25	0.35	0.05	0.03	0.03	0.03	0.03	0.05	0.00	Bal.
2#	0.25	0.35	0.05	0.03	0.03	0.03	0.03	0.05	0.05	Bal.

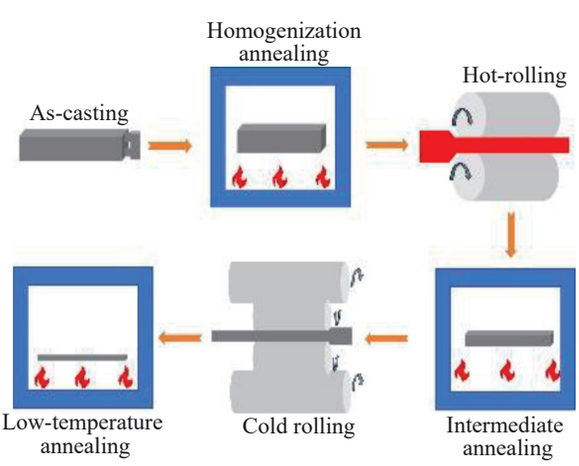

Fig.1 Preparation process of current collector battery aluminum foil

Optical microscope (OM, Leica DMi8), scanning electron microscope (SEM, ZEISS Gemini SEM 300), energy dispersive spectroscope (EDS), and electron backscattered diffractometer (EBSD) analyses with Oxford C-nano probe were used to characterize the microstructures of the samples. Microstructure characterization was performed on the rolling direction-transverse direction plane. Samples were sequentially ground using 600# – 3000# SiC abrasive paper, followed by diamond suspension polishing. Etching was conducted by Keller's reagent (1vol% HF+1.5vol% HCl+ 2.5vol% HNO_3 in H_2O) for 30 – 50 s. After mechanical polishing of 0.3 mm-thick aluminum foil samples, EBSD samples were prepared by electrolytic polishing in a mixed solution of $HClO_4$: C_2H_5OH=1: 9 at power supply voltage of 20 V. EBSD data were analyzed using Aztec Crystal software and HKL Channel 5 software.

Tensile samples were machined along the rolling direction with a gauge length of 50 mm and a width of 12.5 mm. Room-temperature tensile tests were conducted on a universal testing machine based on GB/T 16865-2023 standard. Three samples were tested under each condition for reliability.

Electrical conductivity was measured using an FD-101 eddy current conductometer. The instrument was calibrated with annealed standard blocks (copper and aluminum) before testing. The sample size was 25 mm×25 mm×0.3 mm. Seven points were selected for each sample. Without the maximum and minimum values, the average value of the remaining test results was obtained for the further electrical conductivity analysis.

The aluminum foil was cut into samples of 10 mm×10 mm by a paper cutter. The square aluminum foil sample was ultrasonically cleaned with acetone, anhydrous ethanol, and deionized water in turn. Each cleaning lasted for 10 min. After cleaning and drying, one side of the sample was connected to a copper wire using a conductive adhesive, and the other side was the to-be-tested surface. The treated sample was cold-inlaid. Then, the three-electrode system device was used to test the Tafel polarization curve. The working electrode, the counter electrode, and the reference electrode were the aluminum foil inlaid sample, the metal platinum electrode, and the saturated calomel electrode, respectively. The electrochemical workstation was GAMRY INTERFACE1000E. The electrochemical test was conducted in 3.5wt% NaCl solution.

3 Results and Discussions

3.1 Effect of trace Ce addition on microstructure of as-cast, homogenized, and hot-rolled current collector battery aluminum foils

Fig. 2 compares the as-cast, homogenized, and hot-rolled microstructures of 1# and 2# samples. The as-cast microstructure of 1060 aluminum alloy is mainly composed of α -Al phase and coarse primary phase with continuous distribution. Ce addition reduces the solid solubility of impurity elements and promotes the formation of Ce-containing secondary phases, thereby increasing the overall secondary phase content. Some continuously distributed coarse primary phases are disconnected and become short rod-like and spherical particles. Ce-containing secondary phases serve as heterogeneous nucleation sites for α -Al grains, enabling grain refinement[14]. Grain sizes were quantified using Image-Pro image analysis software. Ce addition refines the average grain size from 41.5 μm to 22.4 μm, corresponding to reduction ratio of 46%. Homogenization treatment dissolves coarse primary phases into the Al matrix, mitigating element segregation. Hot rolling leads to the fracture of coarse secondary phases, inducing precipitation of finely dispersed particles.

3.2 Effect of trace Ce addition on microstructure of cold-rolled and low-temperature annealed current collector battey aluminum foils

Fig.3 shows the microstructures of CR-1#, CR-2#, CR-LA-

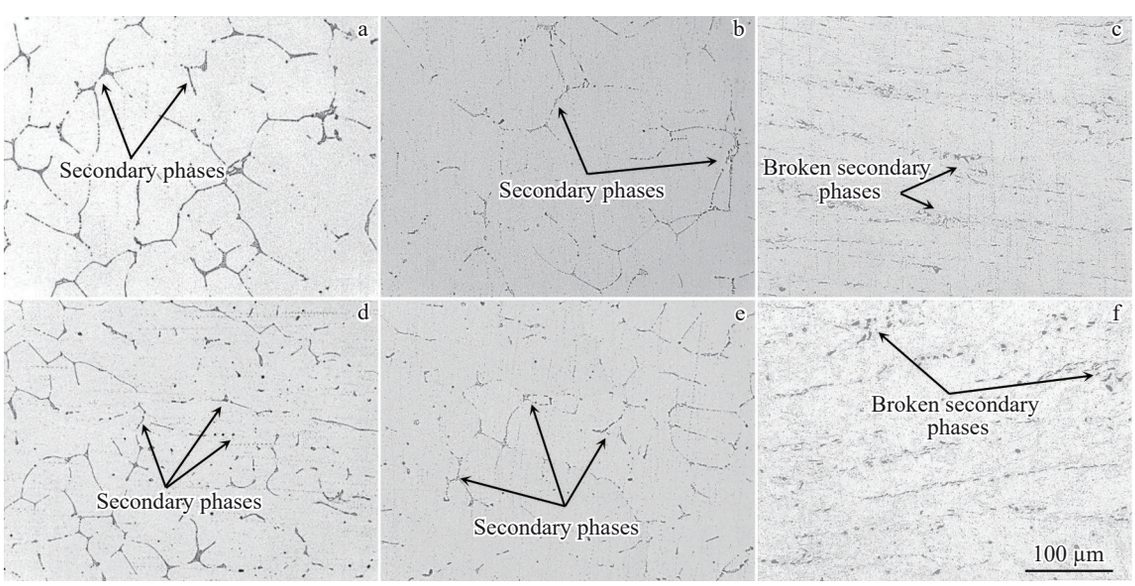

Fig.2 As-cast (a, d), homogenized (b, e), and hot-rolled (c, f) 1# (a–c) and 2# (d–f) samples

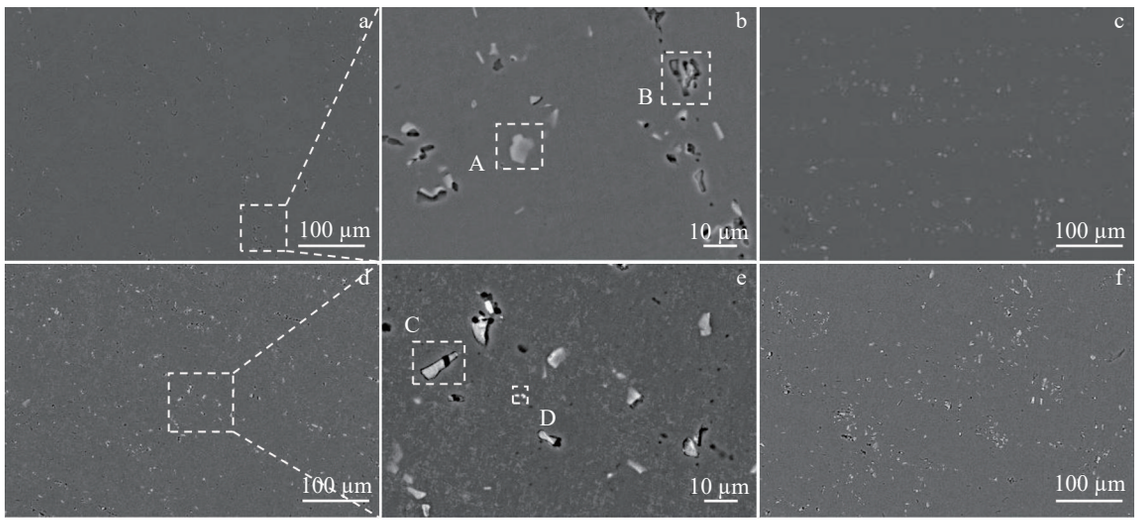

Fig.3 Microstructures of CR-1# (a–b), CR-LA-1# (c), CR-2# (d–e), and CR-LA-2# (f) samples

1#, and CR-LA-2# samples. The composition of regions A–D in Fig. 3b and 3e was analyzed by EDS, and the results are shown in Table 2. Severe cold rolling significantly breaks secondary phases, generating dispersed particles. The addition of RE element Ce to the alloy reduces the solid solubility of the impurity elements in the 1060 aluminum alloy and increases the number of secondary phases, so the number of broken secondary phases in CR-2# sample is larger, and the distribution is more uniform. Fig. 3b and 3e show magnified views of the marked regions of CR-1# and CR-2# samples, respectively. According to EDS results, the secondary phase is mainly gray and gray-black AlFeSi phase. Ce addition promotes the formation of AlCeSi phases, reducing Si solubility in the Al matrix. Low-temperature annealing can matintain the morphology of the secondary phase while slightly increasing the phase density, as shown in Fig. 3c and 3f.

Fig. 4 shows EBSD analyses of CR-1#, CR-2#, CR-LA-1#, and CR-LA-2# samples. Inverse pole figures (IPFs), grain size distributions, and antipolar graphs of all samples are presented in Fig. 4 for analysis. It can be seen that all samples exhibit typical rolling textures with elongated grains parallel to the rolling direction. According to the grain size analysis, the average grain size of the CR-1# sample is 11.2 μm. After adding Ce, the grain size significantly reduces to 10.9 μm, which proves that the addition of RE element Ce has the effect of grain refinement. After annealing, the average grain sizes increases to 13.1 and 12.4 μm for CR-LA-1# and CR-LA-2# samples, respectively. This is because during the annealing process, a small number of grains grow slowly; with the addition of RE element Ce, the grain growth rate of the alloy is restricted, which is closely related to the AlCeSi secondary phase formed by Ce. These precipitates inhibit the grain boundary migration through the Zener pinning effect, thus effectively hindering the grain growth. IPFs show distinct crystal orientation of samples after cold rolling. It can be seen that CR-1# sample is mainly [101] -orientated, and the maximum orientation texture intensity is 8.25. CR-2# sample

Table 2 EDS analysis results of regions A – D in Fig. 3b and 3e (wt%)

Element	Region A	Region B	Region C	Region D
Al	83.54	73.84	74.9	83.21
Fe	13.54	20.48	21.08	-
Si	2.92	5.69	4.02	3.23
Ce	-	-	-	13.56

is mainly [001] -orientated, and the maximum orientation texture intensity is 10.90. After low-temperature annealing treatment, the main orientation of CR-LA-1# sample is still [101], and the maximum orientation texture intensity is 8.09 (lower than that of CR-1# sample), which is manifested as the texture weakening caused by dislocation rearrangement during typical recovery process. The grain orientation of CR-LA-2# sample changes to [111] orientation, and the maximum orientation texture intensity is 10.53. This result demonstrates that Ce addition can modulate the crystallographic evolution during deformation and recovery processes.

Fig. 5 shows the kernel average misorientation (KAM) maps, grain boundary orientation distribution maps, and recrystallization distribution maps of the CR-1#, CR-2#, CR-LA-1#, and CR-LA-2# samples. Severe cold rolling induces high-density dislocation arrays and subgrain formation in all samples. The overall KAM value (θ) of CR-1# sample is 2.26°, and the fraction of low-angle grain boundary (LAGB) is 82.0%. After adding RE element Ce, the overall KAM value and LAGB fraction of CR-2# sample increase to 2.36° and 87.4%, respectively. This enhancement arises from AlCeSi precipitates that impede dislocation motion via slip/climb inhibition, promoting dislocation accumulation and rearrangement into LAGBs. After low-temperature annealing treatment, the overall KAM value of CR-LA-1# and CR-LA-2# samples decreases to 1.82° and 1.96°, respectively, while LAGB fraction of CR-LA-1# and CR-LA-2# samples increases to 84.2% and 90.2%, respectively. This result further confirms that the recovery processes exist during annealing,

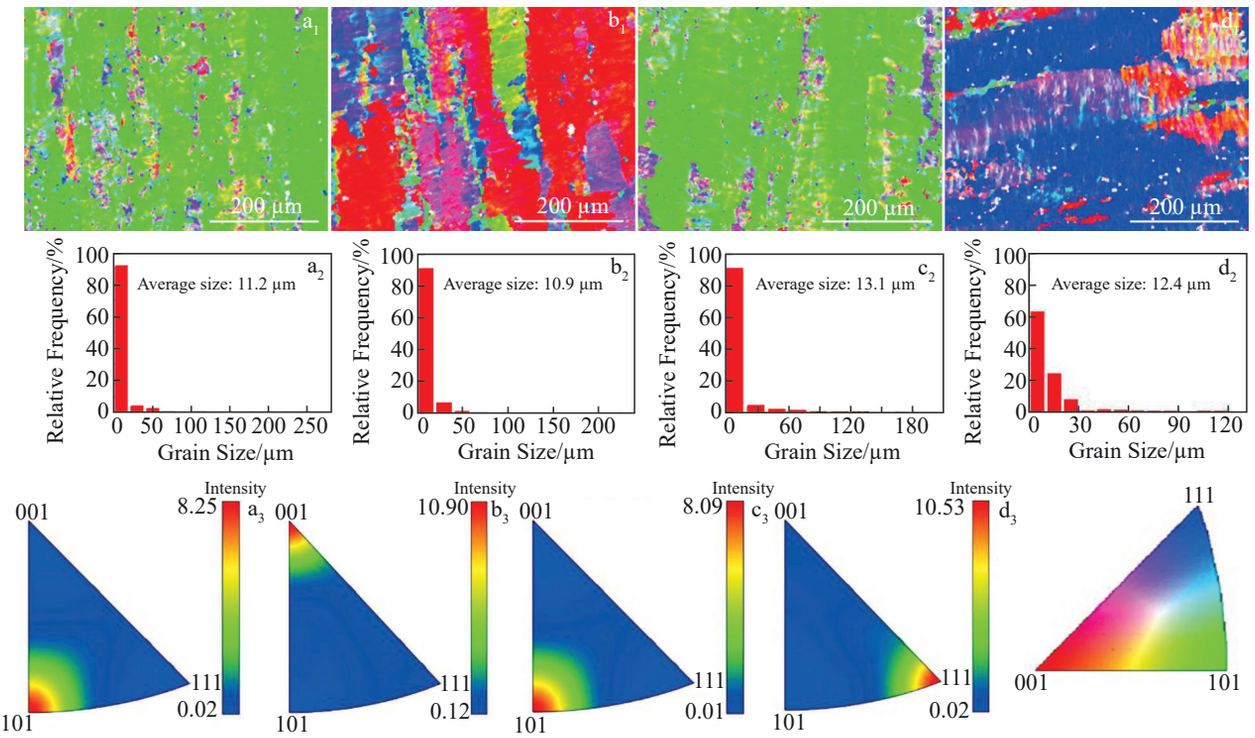

Fig.4 EBSD analyses of CR-1# (a_1–a_3), CR-2# (b_1–b_3), CR-LA-1# (c_1–c_3), and CR-LA-2# (d_1–d_3) samples: (a_1–d_1) IPFs; (a_2–d_2) grain size distributions; (a_3–d_3) antipolar graphs

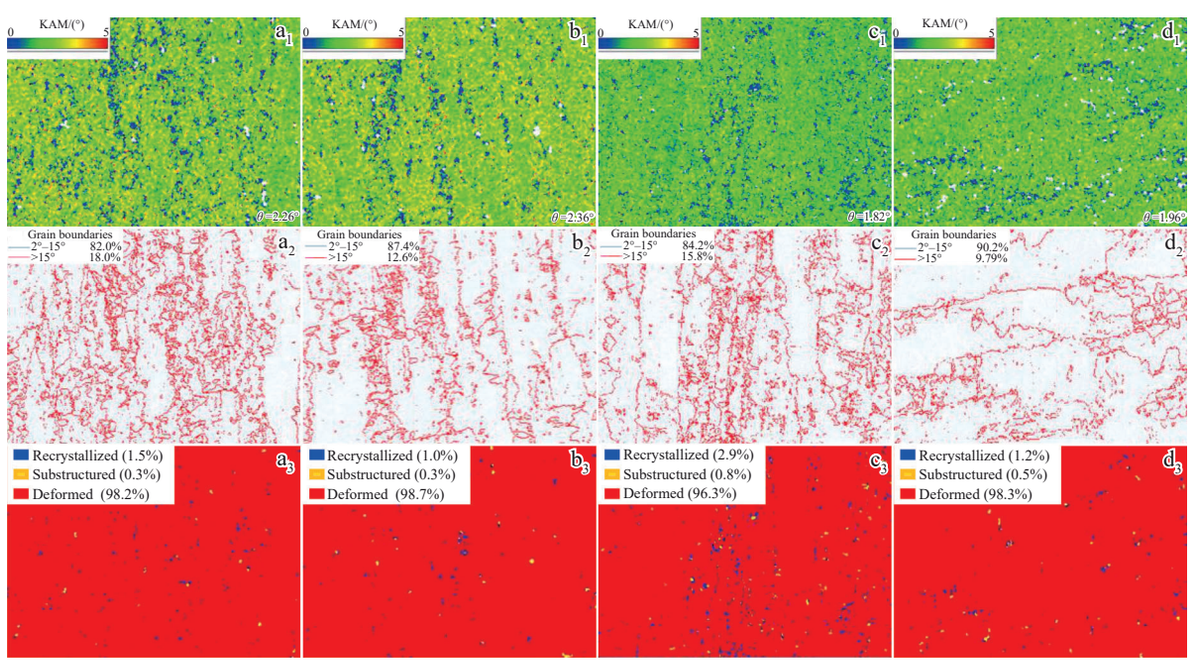

Fig.5 EBSD analyses of CR-1# (a_1–a_3), CR-2# (b_1–b_3), CR-LA-1# (c_1–c_3), and CR-LA-2# (d_1–d_3) samples: (a_1–d_1) KAM maps; (a_2–d_2) grain boundary orientation distribution maps; (a_3–d_3) recrystallization distribution maps

whereas dislocation annihilation occurs. The low-temperature annealing suppresses dynamic recrystallization. In the recovery process, under the action of thermal activation, dislocations will move and rearrange, and dislocation walls perpendicular to the slip direction and those with a certain degree of orientation will produce a more stable subgrain structure. These dislocation walls are LAGBs. Concurrently, Ce-derived precipitates pin the grain boundaries via Zener effect, stabilizing subgrain configurations and increasing LAGB density.

According to Fig. 5a_3 – 5d_3, a large number of deformed grains exist in CR-1# and CR-2# samples, accounting for

98.2% and 98.7%, respectively. Additionally, a small number of recrystallized grains exist, and the proportion of recrystallization of CR-1# and CR-2# samples is 1.5% and 1.0%, respectively. Annealing process increases the proportion of recrystallization to 2.9% and 1.2% for the CR-LA-1# and CR-LA-2# samples, increased by 1.4% and 0.2%, compared with that of CR-1# and CR-2# samples, respectively. Low-temperature annealing reduces dislocation density, leading to partial recrystallization (2.9% recrystallized grains in CR-LA-1# sample). Ce addition reduces the fraction of recrystallization into 1.2%, confirming the Ce recrystallization inhibition effect. It is indicated that the addition of RE element Ce can inhibit the occurrence of recrystallization. The occurrence of recrystallization is due to the heat generated by the contact between the roller surface and the blank surface during the cold rolling process. Because of the local heating of the blank, a slight degree of recrystallization occurs. However, Ce-containing secondary phase particles exist at the grain boundary of the aluminum foils with Ce addition. The secondary phase particles play a pinning role, prevent the migration of grain boundaries, and inhibit the occurrence of recrystallization. In addition, since Ce has a (relatively low) solid solution degree in the aluminum matrix, a small amount of Ce may remain the solid solution state. These residual Ce can exert a solute resistance effect to prevent the migration of grain boundaries.

3.3 Effect of trace Ce on properties of cold-rolled and low-temperature annealed current collector battery aluminum foils

Fig. 6 shows the mechanical properties of the CR-1#, CR-2#, CR-LA-1#, and CR-LA-2# samples. The ultimate tensile strength (UTS) and yield strength (YS) of CR-1# sample are 162 and 147 MPa, respectively; UTS and YS of CR-2# sample are 168 and 151 MPa, respectively. After low-temperature annealing, UTS and YS of the samples reduce. UTS and YS of CR-LA-1# sample reduce to 138 and 125 MPa, respectively, while those of CR-LA-2# decrease to 149 and 137 MPa, respectively. Superior properties of Ce-containing aluminum foils demonstrate the strengthening efficacy of Ce addition. Therefore, after low-temperature annealing, compared with those of CR-1# and CR-2# samples, UTS values are decreased by 24 and 19 MPa, while YS values are reduced by 22 and 14 MPa, respectively.

The strengthening mechanism of mechanical properties is mainly due to the following synergistic effects.

(1) Fine-grain strengthening mechanism: the Hall-Petch formula[22–23] is as follows:

$$\Delta\sigma = \sigma_0 + kd^{-\frac{1}{2}} \quad (1)$$

where σ_0 is the inherent resistance to deformation in the crystal; k is the influence coefficient of the grain boundary on deformation, which is related to the structure of the grain boundary; d is the average grain size. It shows that the addition of RE element Ce improves the strength of the alloy by inhibiting grain growth and reducing grain size.

(2) Dislocation strengthening mechanism: the strength change is caused by work hardening ($\Delta\sigma_{dis}$), and the calculation formula[24–25] is as follows:

$$\Delta\sigma_{dis} = M\alpha_d Gb\sqrt{\rho} \quad (2)$$

where M is the average matrix orientation factor of aluminum (3.06); α_d is a constant related to the material, ranging from 0.15 to 0.5; g is the shear modulus of the aluminum matrix (25.4 GPa at room temperature); b is the value of the Burgers vector (0.286 nm); ρ is the dislocation density. ρ^{GND} is the geometrically necessary dislocation density[26–27], and its calculation formula is as follows:

$$\rho^{GND} = 2\theta_i/ub \quad (3)$$

where θ_i is the average local misorientation based on KAM data; u is the unit length of the point. KAM value in EBSD data shows that the addition of Ce increases the dislocation density and improves the strength of the alloy.

The annealing process was conducted at 200 ℃, which is below the recrystallization threshold of pure aluminum (250–300 ℃). During the low-temperature annealing process, the alloy primarily undergoes recovery rather than complete recrystallization, accompanied by dislocation slip and climb. Dislocations on identical slip planes mutually annihilate through climb mechanisms, thereby reducing the dislocation density. Besides, EBSD analysis reveals the existence of grain growth during annealing. The strength reduction may be attributed to decreased dislocation density and coarsened grains.

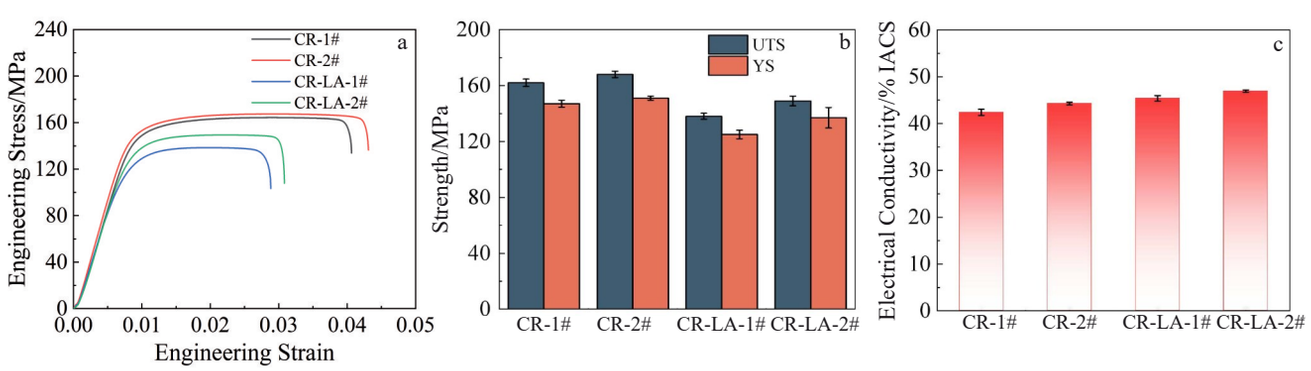

Fig.6 Mechanical properties of CR-1#, CR-2#, CR-LA-1#, and CR-LA-2# samples: (a) engineering stress-engineering strain curves; (b) UTS and YS; (c) electrical conductivity

The electrical conductivity of CR-1#, CR-2#, CR-LA-1#, and CR-LA-2# samples is shown in Fig. 6c. It can be seen that the electrical conductivity of CR-1# and CR-2# samples is 42.40% IACS and 44.28% IACS, respectively. After low-temperature annealing treatment, the electrical conductivity of CR-LA-1# and CR-LA-2# samples increases to 45.38% IACS and 46.94% IACS, respectively. According to Matthiessen's rule[28], the resistivity of aluminum alloy is related to the following factors: (1) intrinsic resistivity of defect-free single-crystal Al; (2) vacancy-induced electron scattering; (3) interface scattering (grain/subgrain boundaries); (4) dislocation and stacking fault contributions; (5) solid solution atom effects; (6) secondary phase particle scattering.

Among them, the most important influence on the electrical conductivity is the solid solution of atoms, resulting in lattice distortion and increasing resistivity. Cold rolling induces grain elongation, forming fibrous structures with abundant LAGBs and intragranular dislocations. In addition, the recrystallization inhibition reduces the high-angle grain boundaries that hinder the movement of electrons, thereby enhancing electron transport. Concurrently, Ce addition promotes the precipitation of Fe and Si impurities into secondary phase compounds. The removal of these solute atoms from the Al matrix reduces lattice strain, thereby diminishing electron scattering. Furthermore, the intrinsic electron scattering of these secondary phases is significantly lower than that of solute atoms in solid solution. Consequently, the enhanced electrical conductivity of the Ce-added foil is primarily attributed to the purification of the aluminum matrix, namely, the reduction in solid solubility of impurity elements. The increase in electrical conductivity after annealing is attributed to the decrease in dislocation density and the increase in the number of LAGBs.

Fig. 7 shows the fracture morphologies of CR-1#, CR-2#, CR-LA-1#, and CR-LA-2# samples. All samples exhibit cleavage planes and dimples, confirming a typical mixed-mode fracture mechanism. Ce addition increases the dimple density and depth, which is attributed to the grain refinement effect.

Fig. 8 shows Tafel polarization curves of CR-1#, CR-2#, CR-LA-1#, and CR-LA-2# samples in 3.5wt% NaCl solution. The corrosion potential (E_{corr}) and corrosion current density (I_{corr}) of the alloy were calculated by the extrapolation method.

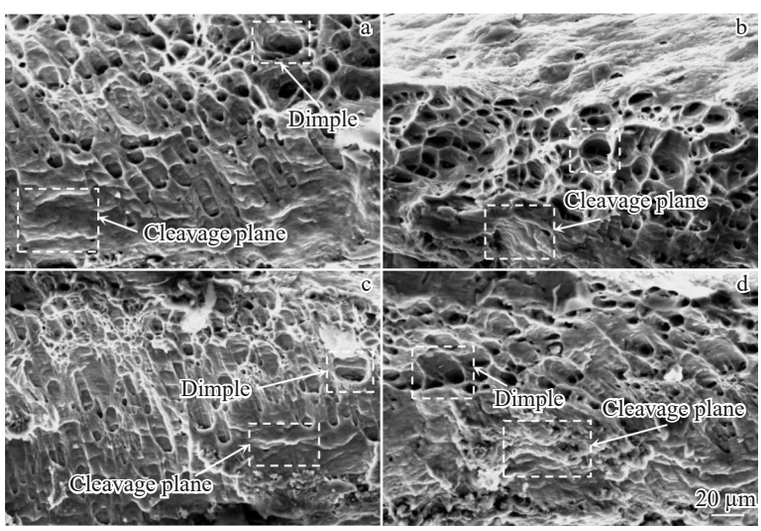

Fig.7 Fracture morphologies of CR-1# (a), CR-2# (b), CR-LA-1# (c), and CR-LA-2# (d) samples

Table 3 shows the corresponding E_{corr} and I_{corr} results of all samples. The corrosion potentialsl (E_{corr}) of CR-1#, CR-2#, CR-LA-1#, and CR-LA-2# samples are −730, −567, −707, and −501 mV vs. SCE, respectively. Ce addition induces a significant positive shift in corrosion potential. Generally, the higher the E_{corr}, the better the chemical stability, i.e., the better the corrosion resistance[29]. The increase in corrosion potential may be due to the addition of RE element Ce, the grain refinement effect, the decrease in the proportion of high-angle grain boundaries, and the reduction in intergranular corrosion channels. It is reported that the finer the grains, the better the corrosion resistance[30]. Although annealing causes minor grain coarsening, residual stress release dominates, thereby reducing corrosion sensitivity by diminishing galvanic couples at grain boundaries.

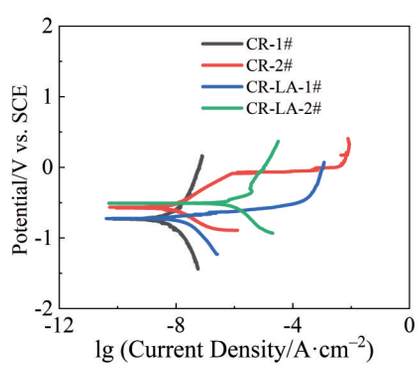

Fig.8 Tafel polarization curves of CR-1#, CR-2#, CR-LA-1#, and CR-LA-2# samples in 3.5wt% NaCl solution

Table 3 Fitting results of Tafel polarization curves for CR-1#, CR-2#, CR-LA-1#, and CR-LA-2# samples

Sample	E_{corr}/mV vs. SCE	I_{corr}/A·cm^{-2}
CR-1#	−730	2.03×10^{-7}
CR-2#	−567	5.49×10^{-8}
CR-LA-1#	−707	1.35×10^{-6}
CR-LA-2#	−501	0.74×10^{-6}

4 Conclusions

1) Trace Ce addition forms AlCeSi intermetallic phases with matrix Si, which reduces the solubility of impurity elements and reduces the grain size by heterogeneous nucleation. During cold rolling, Ce-rich secondary phase particles at grain boundaries induce Zener pinning, inhibiting the dislocation annihilation via slip/climb and increasing the dislocation density. Subsequent low-temperature annealing reduces dislocation density, leading to partial recrystallization (2.9% recrystallized grains in CR-LA-1# sample). Ce addition reduces the fraction of recrystallization into 1.2%, confirming the Ce recrystallization inhibition effect.

2) UTS and YS of CR-1# sample are 162 and 147 MPa, respectively; UTS and YS of CR-2# sample are 168 and 151 MPa, respectively. After low-temperature annealing, UTS and YS of the samples reduce. UTS and YS of CR-LA-1# sample reduce to 138 and 125 MPa, respectively, while those of CR-LA-2# decrease to 149 and 137 MPa, respectively. After low-temperature annealing, compared with those of CR-1# and CR-2# samples, UTS values are decreased by 24 and 19 MPa, while YS values are reduced by 22 and 14 MPa, respectively. Ce addition enhances the strength via coordinated grain refinement and dislocation strengthening mechanisms.

3) Ce-modified foil exhibits enhanced electrical conductivity. The electrical conductivity of CR-1# and CR-2# samples is 42.40% IACS and 44.28% IACS, respectively. After low-temperature annealing treatment, the electrical conductivity of CR-LA-1# and CR-LA-2# samples increases to 45.38% IACS and 46.94% IACS, respectively. This enhancement primarily stems from Ce-induced reduction in impurity solid solubility within the Al matrix.

4) Ce addition induces a positive shift in corrosion potential, demonstrating enhanced corrosion resistance. This improvement primarily stems from Ce-induced grain refinement. The process of annealing at 200 ℃ for 6 h releases residual stress, reducing corrosion susceptibility by diminishing galvanic couples at grain boundaries.

References

1 Peng Z X, Ding D Y, Zhang W L *et al*. *Materials*[J], 2022, 15(15): 5126

2 Zhu P, Gastol D, Marshall J *et al*. *Journal of Power Sources*[J], 2020, 485: 229321

3 Li J X, Sun S, Zhang X *et al*. *ACS Applied Energy Materials*[J], 2025, 8(6): 3826

4 Otaegui L, Goikolea E, Aguesse F *et al*. *Journal of Power Sources*[J], 2015, 297: 168

5 Wang C C, Lin Y C, Chiu K F *et al*. *Chemistry Select*[J], 2017, 2(16): 4419

6 Zhang Y, Li W G, Hu Y J *et al*. *Metals*[J], 2024, 14(6): 617

7 Yang X, Ding D Y, Xu Y X *et al*. *Metals*[J], 2019, 9(6): 706

8 Bonatti C, Mohr D. *Materials Science and Engineering A*[J], 2016, 654: 329

9 Wang J, Li F G. *Materials*[J], 2023, 16(13): 11

10 Hao J P, Yan L M, Dai Y X. *Reviews on Advanced Materials Science*[J], 2023, 62(1): 20230345

11 Hu G Y, Zhu C J, Xu D F *et al*. *Journal of Rare Earths*[J], 2021, 39(2): 208

12 Huang Y C, Xia L F, Yang H B *et al*. *Materials*[J], 2025, 18(3): 648

13 Wang Xiaobo, Rong Li, Huang Hui *et al*. *Rare Metal Materials and Engineering*[J], 2024, 53(1): 250 (in Chinese)

14 Cui X M, Wang Z W, Cui H *et al*. *Materials Research Express*[J], 2023, 10(8): 086511

15 Li X, Li A M, Qin X *et al*. *Materials*[J], 2024, 17(16): 4141

16 Yu J Z, Wang C X, Liang R D *et al*. *Integrated Ferroelectrics*[J], 2023, 236(1): 40

17 Chen L, Luo Y T, Zhou Q S *et al*. *Transactions of Nonferrous Metals Society of China*[J], 2025, 35(7): 2148

18 Qi Zhongyi, Wang Bo, Jiang Hongxiang *et al*. *Acta Physica Sinica*[J], 2024, 73(7): 076401 (in Chinese)

19 Zhang Y L, Wei F, Mao J *et al*. *Materials Characterization*[J], 2019, 158: 109963

20 Yang Huaide, Long Siyuan, Zhu Shuqing *et al*. *Rare Metal Materials and Engineering*[J], 2016, 45(1): 187 (in Chinese)

21 Czerwinski F. *Journal of Materials Science*[J], 2020, 55(12): 24

22 Hansen N. *Scripta Materialia*[J], 2004, 51(8): 801

23 Wang Z J, Zhang M, Zhang Q Y *et al*. *Rare Metal Materials and Engineering*[J], 2020, 49(10): 3402

24 Zhou S Y, Wang J Y, Yang G *et al*. *Materials Science and Engineering A*[J], 2022, 860: 17

25 Wang L Y, Liu C Y. *Materials Science and Engineering A*[J], 2024, 915: 10

26 Li Z L, Liu C Y. *Intermetallics*[J], 2025, 176: 108559

27 Wang H L, Ma J, Yuan M N *et al*. *Materials Today Communications*[J], 2022, 33: 104605

28 Wang M M, Zhou Y, Lv H Y *et al*. *Journal of Alloys and Compounds*[J], 2021, 882: 160692

29 Yang X T, Li X Q, Yang Q B *et al*. *Surface & Coatings Technology*[J], 2020, 385: 125359

30 Zhong S Y, Zhang D F, Wang Y Q *et al*. *Journal of Materials Science & Technology*[J], 2022, 128: 44

添加Ce对1060集流体电池铝箔组织和性能的影响

赵星驰[1,2]，李瑞雪[1]，李芃昊[3]，李婉莹[4]，李继林[1,2]，姜　博[1]，杜新伟[5]

(1. 哈尔滨理工大学 材料科学与化学工程学院，黑龙江 哈尔滨 150080)

(2. 广东省科学院 新材料研究所，广东 广州 510640)

(3. 广州涉外经济学院 信息工程学院，广东 广州 510540)

(4. 广州铱尹新材料科技有限公司，广东 广州 510640)

(5. 乳源东阳光优艾希杰精箔有限公司，广东 韶关 512600)

摘　要：选用商业用1060集流体电池铝箔作为基体，添加稀土元素Ce，采用熔炼、除气净化、过滤处理、热轧、冷轧等工艺处理掺Ce铝箔，分析Ce添加对1060集流体电池铝箔的影响规律和机制。结果表明：在1060集流体电池铝箔中形成了AlCeSi金属间化合物相，其作为异质形核核心，能够细化晶粒；在冷轧变形过程中，晶界处含有Ce的第二相粒子产生强Zener钉扎效应，增加位错密度，抑制再结晶。细晶强化和位错强化协同强化，改善了铝箔的力学性能。添加Ce还能够降低基体中杂质元素的固溶度，改变晶格畸变散射，提高其导电性。添加稀土元素Ce，能够细化晶粒，促进腐蚀电位沿正向移动，进而提高耐腐蚀性能。

关键词：集流体电池铝箔；微量Ce合金化；轧制工艺；导电性能；耐腐蚀性能

作者简介：赵星驰，男，2000年生，硕士生，哈尔滨理工大学材料科学与化学工程学院，黑龙江 哈尔滨 150080，E-mail：1445876921@qq.com